A Necessarily Incomplete Review of Electromagnetic Finite Element Particle-in-Cell Methods

Omkar H. Ramachandran, *Graduate Student Member, IEEE*, Leo C. Kempel, *Fellow, IEEE*, John P. Verboncoeur, *Fellow, IEEE*, and B. Shanker, *Fellow, IEEE*

***Abstract*— While finite-difference time-domain methods have long been the foundational basis for particle-in-cell (PIC) codes, there has been increasing momentum in developing a suite of finite element-based PIC methods. The beauty of finite difference-based methods is that it is easily cast within the correct mathematical framework to represent fields, fluxes, currents, and charges. However, more importantly, these methods are cost-effective. In the intervening years, since finite difference methods were developed, the state of the art of field modeling has shifted rather dramatically. Indeed, the most popular and trusted field simulators are based on the finite element method (FEM), thanks, in large part, to the discovery of the correct function spaces for quantities of interest for Maxwell's equations, but also the flexibility that it brings to modeling geometry with the ability to refine in space and numerical order to better capture the underlying physics. Together with time-stepping schemes that are unconditionally stable, these methods provide the framework necessary to correctly capture the nuance of the physical evolution with high fidelity. The intent of this article is to review advances in electromagnetic finite element PIC (EM-FEMPIC). We will address the progress made in fundamental challenges in such a method for charge conservation to more programmatic ones, such as computational complexity.**

***Index Terms*— Coulomb gauge, finite element method (FEM), Gauss' laws, implicit time stepping, particle-in-cell (PIC), quasi-Helmholtz decomposition, unconditionally stable.**

I. Introduction

The electromagnetic particle-in-cell (EM-PIC) method is widely used as a solution technique to model the physics of moving charged particles. Primarily, these schemes have a number of advantages over other fluid-based simulation techniques, including a fundamentally simple solution algorithm, the ability to model physics over a wide range of frequency and energy regimes, and being robust and accurate in the modeling of complex devices. As a result, EM-PIC finds widespread use in modeling devices, such as particle accelerators and high-power microwave devices, and plasma processing applications, such as high-precision etching and sterilization of medical implements [1], [2], [3]. Given the demand for high-fidelity simulation tools, as the geometry becomes more complex, significant effort has been expended into the analysis and optimization of PIC methods over the last few decades. An easy way to see the advance is to compare our discussion to a review in the context of high-power microwave devices from 2001 [4]: Note that the easy scalability of the solution algorithm has meant that PIC methods have gone from simulating a few hundred particles over a 1-D grid to a parallel implementation capable of evolving well over ten million particles to one billion particles in fully resolved 3-D.

The goals of this review are to provide a rigorous overview of the advances made in the analysis and development made in implicit electromagnetic finite element PIC (EM-FEMPIC) solvers in recent years. Specifically, this review will address the following.

1) A brief overview of the various methods and formulations that exist in the PIC literature.
2) The current state of the art as it pertains to EM-FEMPIC and where the field stands at this moment in time.
3) Provide a brief outline of the mathematical formalism involved with EM-FEMPIC methods, particularly in relation to basis function choices and their effects on charge conservation.
4) Highlight areas for future development and advances in the field.

The field of EM-FEMPIC is extensive, and as such, we note that this review will not delve into interesting topics within this field, including the following.

1) The history and evolution of PIC schemes and development.
2) PIC methods that do not make use of full-wave EM solvers, i.e., electrostatic simulation [5].
3) Other conformal solution schemes, including those based on finite-difference time domain (FDTD), discrete exterior calculus, and so on. A good overview of these is provided here [6].

The remainder of this article will be structured as follows. Sections II and IV will introduce a general problem setup and briefly review the state of the art of various PIC methods.

Manuscript received 17 November 2022; revised 19 February 2023; accepted 27 February 2023. Date of publication 28 March 2023; date of current version 22 August 2023. The review of this article was arranged by Senior Editor S. J. Gitomer. *(Corresponding author: Omkar H. Ramachandran.)*

Omkar H. Ramachandran and John P. Verboncoeur are with the Department of Electrical and Computer Engineering, Michigan State University, East Lansing, MI 48824 USA (e-mail: ramach21@egr.msu.edu).

Leo C. Kempel is with the Department of Electrical and Computer Engineering at Michigan State University, East Lansing, MI 48823 USA.

B. Shanker was with the Department of Electrical and Computer Engineering, Michigan State University, East Lansing, MI 48824 USA. He is now with the Department of Electrical and Computer Engineering, The Ohio State University, Columbus, OH 43210 USA.

Color versions of one or more figures in this article are available at https://doi.org/10.1109/TPS.2023.3257165.

Digital Object Identifier 10.1109/TPS.2023.3257165

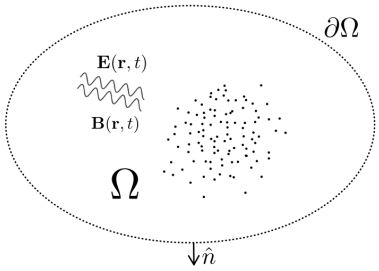

Fig. 1. General schematic of the simulation domain.

Section III will then go over the basic formalism associated with building a finite element-based solution scheme. Section V-A will then review the spatial discretization used within a typical EM finite element solver and how they contribute to charge conservation. After this, Section V-B will analyze various choices of basis functions and the impact that they have on charge conservation. In particular, we will go over a rigorous analysis that demonstrates the conditions under which satisfaction of Gauss' electric law is achieved by default in explicit time-evolution schemes and how it is typically not satisfied in an implicit method. We will then go over the reformulation of Ampere's law suggested in [7] and demonstrate how this change preserves charge. Section V-D will then detail the formulation of the quasi-Helmholtz scheme that explicitly enforces the Coulomb gauge, and thereby, both satisfy charge conservation and mitigate the spurious null space excitations that are endemic in implicit EM solvers.

II. Problem Statement

Consider a region $\Omega \in \mathbb{R}^3$ bounded by a surface $\partial\Omega$ containing a single charged species as shown in Fig. 1. This region is subjected to an external field due to which the charged species accelerate and, in turn, produce spatially and temporally varying electric and magnetic fields denoted by $\mathbf{E}(\mathbf{r},t)$ and $\mathbf{B}(\mathbf{r},t)$, respectively, with $\mathbf{r} \in \Omega$ and $t \in [0,\infty)$. The dynamics of the particles in phase space can be represented by a distribution function [phase space distribution function (PSDF)] $f(t,\mathbf{r},\mathbf{v})$ that follows the Vlasov equation:

$$\partial_t f(t,\mathbf{r},\mathbf{v}) + \mathbf{v}\cdot\nabla f(t,\mathbf{r},\mathbf{v}) + \frac{q}{m}[\mathbf{E}(\mathbf{r},t)+\mathbf{v}\times\mathbf{B}(\mathbf{r},t)]\cdot\nabla_v f(t,\mathbf{r},\mathbf{v}) = 0. \quad (1)$$

In what follows, we assume that the background media in Ω is free space. As a result, we denote the permittivity and permeability of free space by ϵ_0 and μ_0, respectively, and the speed of light by c. Finally, we will also assume that the system is quiescent for $t \le 0$.

III. Fundamental Equations and Particle-in-Cell Approximation

As is traditionally done in PIC schemes, we elect to not solve (1) directly, but, rather, we represent the charge and current distributions in Ω using the moments of the PSDF through $\rho(\mathbf{r},t) = q\int_\Omega f(t,\mathbf{r},\mathbf{v})d\mathbf{v}$ and $\mathbf{J}(\mathbf{r},t) = q\int_\Omega \mathbf{v} f(t,\mathbf{r},\mathbf{v})d\mathbf{v}$. Representing these moments using N_p macroparticles, one can evolve their positions and velocity together with Maxwell's equations. Assuming a shape function $S(\mathbf{r})$, we obtain

$$\rho(\mathbf{r},t) = q\sum_{p=1}^{N_p} S(\mathbf{r}-\mathbf{r}_p(t)) \quad (2a)$$

$$\mathbf{J}(\mathbf{r},t) = q\sum_{p=1}^{N_p} \mathbf{v}_p(t) S(\mathbf{r}-\mathbf{r}_p(t)) \quad (2b)$$

where $\mathbf{r}_p(t)$ and $\mathbf{v}_p(t)$ refer to the positions and velocities as functions of time of the pth macroparticle. The evolution of the fields $\mathbf{E}(\mathbf{r},t)$ and $\mathbf{B}(\mathbf{r},t)$ over space and time within Ω follows Maxwell's equations, given by

$$\nabla\times\mathbf{E}(\mathbf{r},t) = -\partial_t\mathbf{B}(\mathbf{r},t) \quad (3a)$$

$$\nabla\times\mu_0^{-1}\mathbf{B}(\mathbf{r},t) = \mathbf{J}_i(\mathbf{r},t)+\mathbf{J}(\mathbf{r},t)+\epsilon_0\partial_t\mathbf{E}(\mathbf{r},t) \quad (3b)$$

where $\mathbf{J}_i(\mathbf{r},t)$ describes impressed currents within Ω. Furthermore, the solutions to the curl equations in (3) also need to satisfy Gauss' laws

$$\nabla\cdot\epsilon_0\mathbf{E}(\mathbf{r},t) = \rho_i(\mathbf{r},t)+\rho(\mathbf{r},t) \quad (4a)$$

$$\nabla\cdot\mathbf{B}(\mathbf{r},t) = 0 \quad (4b)$$

where $\rho_i(\mathbf{r},t)$ are impressed charges. In what follows, we will assume that both the impressed current and the corresponding charge densities are zero. If they are not, it is trivial to include them in the analysis framework rubric described in Section IV.

As usual, boundary conditions need to be imposed on $\mathbf{E}(\mathbf{r},t)$ and $\mathbf{B}(\mathbf{r},t)$ on sections of the outer boundary $\partial\Omega$ to ensure unique solutions. These are assumed to be either Dirichlet, Neumann, or impedance boundary conditions on nonoverlapping surfaces $\partial\Omega_D$, $\partial\Omega_N$, and $\partial\Omega_I$, with $\partial\Omega = \partial\Omega_D+\partial\Omega_N+\partial\Omega_I$, and are defined as follows:

$$\hat{n}\times\mathbf{E}(\mathbf{r},t) = \Psi_D(\mathbf{r},t) \text{ on } \Omega_D \quad (5a)$$

$$\hat{n}\times\mu^{-1}\mathbf{B}(\mathbf{r},t) = \Psi_N(\mathbf{r},t) \text{ on } \Omega_N \quad (5b)$$

$$\hat{n}\times\mu^{-1}\mathbf{B}(\mathbf{r},t) - Y\hat{n}\times\hat{n}\times\mathbf{E}(\mathbf{r},t) = \Psi_I(\mathbf{r},t) \text{ on } \Omega_I \quad (5c)$$

where the functions $\Psi_D(\mathbf{r},t)$, $\Psi_N(\mathbf{r},t)$, and $\Psi_I(\mathbf{r},t)$ refer to the imposed Dirichlet, Neumann, and impedance boundary conditions, respectively.

The evolution of the macroparticles in space and time is determined by solving for the relativistic equations of motion with the acceleration determined by the Lorentz force. This yields the following coupled system of equations for ordinary differential equations (ODEs) for $\mathbf{v}_p(t)$ and $\mathbf{r}_p(t)$:

$$\frac{d\gamma_p\mathbf{v}_p(t)}{\mathrm{dt}} = \frac{q}{m}\left[\mathbf{E}(\mathbf{r}_p(t),t)+\mathbf{v}_p(t)\times\mathbf{B}(\mathbf{r}_p(t),t)\right] \quad (6a)$$

$$\frac{d\mathbf{r}_p(t)}{\mathrm{dt}} = \mathbf{v}_p(t). \quad (6b)$$

IV. Contemporary Solution Methods for Particle-in-Cell

In EM-PIC, the solution cycle typically consists of two parts: a full-wave electromagnetic field solver to update fields within the simulation domain as a function of space and time used in conjunction with a Newton solver that evolves the particle trajectories in response to these fields. These two

steps need to be done self-consistently in order to simulate the physics of the moving charges.

Due to the simplicity of this scheme and its ability to generate accurate solutions, many different combinations of field and particle solvers have been developed. The remainder of this section will provide a brief overview of these methods.

A. Finite-Difference Time Domain

The oldest and by far the most well-analyzed EM-PIC method involves using an FDTD stencil to update the fields along with a modified leapfrog stencil developed by Boris [8] to evolve the particles. The simplest FDTD methods work primarily by breaking up the simulation domain into a Yee grid [9] and placing electric and magnetic field quantities on the primal and dual meshes, respectively. The history of FDTD-based PIC methods is vast and well-studied; we refer the reader to these reviews—and the references therein—for a deeper explanation of the method [10], [11], [12].

One of the fundamental bottlenecks with using an FDTD-based method is the relative difficulty involved with representing curved surfaces, leading to well-known "staircasing" errors, as documented in [13], [14], [15], [16], and [17]. To mitigate this, several "conformal" methods have been proposed and analyzed. While the earliest implementations were limited to straight-edged domains [18], [19], [20], [21], these were quickly extended to curved/curvilinear boundaries [22], [23], [24] with several updates proposed to resolve problems with stability [25] and better incorporation of dielectric near a curved interface [26], [27].

Currently, popular implementations of conformal FDTD include methods that modify boundary cells with an appropriate polygon and enforce the correct boundary condition on the fields. The best exponent of this is the Dey–Mittra scheme [28], [29], [30], [31], [32], with subsequent contributions resolving issues with the maximum allowable step size [33], [34], [35], [36], allowing the method to be used without a prohibitively small stability constraint. Likewise, irregular interfaces separating dielectrics have also been analyzed using various weighting tricks and constraints [26]. Furthermore, symplectic, simple conformal PIC (SC-SPIC) method formulations have been developed and shown to efficiently handle curvilinear boundaries [37]. We note, at this point, that this is only a small sampling of the methods that exist to deal with applying FDTD to systems with curved interfaces. We refer the reader to this review for a deeper explanation [6].

B. Finite Volume Methods

Similar to FDTD, finite-volume time-domain (FVTD) methods have also been used extensively to solve general electromagnetic problems, with the earliest implementations as in [38], [39], and [40]. Improvements in higher order representation and extension to higher order grids [41] and stencils that exactly preserve charge [42], [43] and energy [44] were achieved in recent years. FVTD-based solvers have been implemented in conjunction with particle pushers in a PIC scheme, notably including charge-conserving schemes with higher order particle evolution in time [45], [46] and drift diffusion-based methods for simulating glow discharges [47], along with a number of updates for charge correction [48], [49], [50] and modeling stochastic collisions [51], [52], [53].

C. Discontinuous Galerkin Methods

In a similar manner, there exists a significant body of work on using discontinuous Galerkin time-domain (DGTD) methods for PIC [54], [55], [56], [57]. DGTD-PIC methods have been used with success to simulate a number of particle systems [58], [59], [60] in addition to Vlasov–Poisson [61], [62], [63] and Vlasov–Ampere systems [64], [65].

V. Finite Element Methods

While the aforementioned methods have been widely used, we note that, over the past two plus decades, the state of the art of finite element methods (FEMs) in electromagnetics has grown by leaps and bounds [66]. Today, it is at a state where it has become the de facto modeling algorithm used by commercial software companies. With this background, it follows that FEM could potentially be a robust tool for PIC, and an examination of the bottlenecks and methods developed to overcome them constitutes the rest of this article. The viability of finite element field solver was proven through a series of seminal papers [67], [68], [69], [70], which demonstrated both the constraints on charge mapping and basis function representation that enabled an FEM solver to be integrated with a PIC scheme without breaking important conservation properties. These results in totality are often denoted as structure-preserving methods. These results have been augmented with the development of symplectic formulation methods to better conserve charge and energy [71], [72]. By and large, the methods developed rely on the explicit field and particle updates, as these naturally conserve charge. Unfortunately, explicit methods are conditionally stable, and the stability criterion is related to the finest feature in the mesh. In other words, the time step size that can be used is governed by the smallest mesh element. This implies that the analysis of geometrically complex systems requires significant computational resources. Indeed, this feature is shared by all other methods discussed thus far. An obvious remedy is an implicit scheme that is unconditionally stable. Such schemes for FEM are well known [73]. The main question is how can one adapt such methods to satisfy the conservation of quantities necessary for a PIC scheme. These were addressed in a collection of recent papers [7], [74], [75], wherein a collection of fundamental rules were prescribed. These need to be satisfied by the EM solver and particle evolution scheme for the charge to be innately conserved without needing expensive postprocessing measures, such as divergence cleaning. The framework established through the aforementioned papers has been expanded further to more efficiently solve systems with narrowband field responses by implementing a time-marching scheme built around envelope tracking [76], higher order basis sets [77], domain decomposition to glean efficiency [78], and relativistic motion [79]. Fundamentally, Crawford et al. [74] and Ramachandran et al. [76] identified

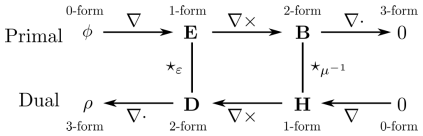

Fig. 2. Overview of the de-Rham complex and the discrete operations needed to map functions in one function space to another.

the failure to conserve charge as being the result of inconsistent choices of representation and testing functions (in space and time) in the discretization of Ampere's and Gauss' laws. This understanding led to the proposal of a slight modification to the current term in Ampere's law, which was shown to ensure charge conservation to machine precision [7]. However, implicit time-stepping schemes come with their own challenge; they admit null spaces that correspond to a dc field (in the case of Maxwell solvers) or a time-growing dc field (in the case of wave equation field solvers). The existence of these is clearly evident in [75]. Overcoming this bottleneck involved a fundamental change in spatial representation and through the use of a quasi-Helmholtz decomposition [75].

In what follows, we will review each of these aspects of an EM-FEMPIC scheme. These methods have been applied to a variety of problems, and results can be found in [7], [67], [68], [75], [76], [80], and [81].

A. Discretization in Space

FEM discretization of (3) requires choosing appropriate spatial basis functions that respect the unique continuity conditions demanded by Maxwell's equations, namely, the tangential continuity of $\mathbf{E}(\mathbf{r}, t)$ and the normal continuity of $\mathbf{B}(\mathbf{r}, t)$. Traditionally, these conditions have been met by choosing Whitney edge and face basis functions that live on and appropriately transform following the de-Rham complex (as depicted in Fig. 2). Assuming a tetrahedral discretization of Ω with N_e and N_f faces, $\mathbf{E}(\mathbf{r}, t)$ and $\mathbf{B}(\mathbf{r}, t)$ are interpolated in space as

$$\begin{aligned}\mathbf{E}(\mathbf{r}, t) &= \sum_{i=1}^{N_e} e_i(t)\mathbf{W}_i^1(\mathbf{r})\\ \mathbf{B}(\mathbf{r}, t) &= \sum_{i=1}^{N_f} b_i(t)\mathbf{W}_i^2(\mathbf{r})\end{aligned} \tag{7}$$

where $\mathbf{W}_i^1(\mathbf{r}) \in H(\text{curl}; \Omega)$ and $\mathbf{W}_i^2(\mathbf{r}) \in H(\text{div}; \Omega)$ represent the Whitney edge function defined on the ith edge and Whitney face function defined on the tth face, respectively. The function spaces $H(\text{curl}; \Omega)$ and $H(\text{div}; \Omega)$ are defined as

$$\begin{aligned}H(\text{curl}; \Omega) &= \left\{\mathbf{u} \in \mathbf{L}^2(\Omega); \nabla \times \mathbf{u} \in \mathbf{L}^2(\Omega)\right\}\\ H(\text{div}; \Omega) &= \left\{\mathbf{u} \in \mathbf{L}^2(\Omega); \nabla \cdot \mathbf{u} \in \mathbf{L}^2(\Omega)\right\}\end{aligned} \tag{8}$$

where $\mathbf{L}^2(\Omega)$ refers to the space of square integrable functions on Ω. Further details on mixed finite elements can be found [82], [83], [84], [85], [86], and references therein. One can obtain a discrete system of equations by Galerkin testing, resulting in the following matrix ODE to solve for the vector of field coefficients $\bar{B}(t)$ and $\bar{E}(t)$ at a given instance of time:

$$\left[\bar{\bar{S}}\right] \cdot \begin{bmatrix}\bar{B}(t)\\ \bar{E}(t)\end{bmatrix} + \left[\bar{\bar{M}}\right] \cdot \begin{bmatrix}\partial_t \bar{B}(t)\\ \partial_t \bar{E}(t)\end{bmatrix} = \bar{\bar{F}} \tag{9}$$

where the various matrix definitions are given as follows:

$$\begin{aligned}\left[\bar{\bar{S}}\right] &= \begin{bmatrix}0 & [\nabla\times]\\ -[\nabla\times]^T & 0\end{bmatrix}\\ \left[\bar{\bar{M}}\right] &= \begin{bmatrix}\left[\star_{\mu^{-1}}\right] & 0\\ 0 & [\star_\epsilon]\end{bmatrix}\\ \bar{\bar{F}} &= -\begin{bmatrix}0\\ \dfrac{\bar{J}(t)}{\epsilon_0}\end{bmatrix}.\end{aligned} \tag{10}$$

Furthermore, $\bar{B}(t) = [b_1(t), \ldots, b_{N_f}(t)\ ]^T$, $\bar{E}(t) = [e_1(t), \ldots, e_{N_e}(t)]^T$, and $\bar{J}(t) = [j_1(t), \ldots, j_{N_e}(t)]^T$, where $j_j(t) = \langle \mathbf{W}_j^{(1)}, \tilde{\mathbf{J}}(\mathbf{r}_s, t)\rangle$. One can likewise trivially formulate a wave-equation solver for just the electric or magnetic fields, as done in [7]. The matrices in (10) are defined in the Appendix.

B. Charge Conservation and Temporal Discretization

To convert (9) into a discrete update stencil in time, one has to choose representation and testing functions in time as done in the spatial setup. In general, the vector of coefficients $\bar{B}(t)$ and $\bar{E}(t)$ can be interpolated by a set of temporal basis functions $N_n(t)$. We exploit an abuse of notation to represent discrete samples of the electric field and the magnetic flux density at timestep t_n as $\bar{E}(t_n)$ and $\bar{B}(t_n)$, respectively. Thus, at any given time t

$$\begin{pmatrix}\bar{B}(t)\\ \bar{E}(t)\end{pmatrix} = \sum_{n=0}^{N_t} N_n(t)\begin{pmatrix}\bar{B}(t_n)\\ \bar{E}(t_n)\end{pmatrix}. \tag{11a}$$

We can obtain a discrete marching scheme by testing (9) by an appropriate function $W_n(t)$. Both $N_n(t)$ and $W_n(t)$ are assumed to have compact support. Our goal, in this section, is to examine the consequences of charge-conserving PIC of choosing various forms of time representation and testing. In the continuous world, solutions to Faraday's/Ampere's laws will automatically satisfy Gauss' electric and magnetic laws. Failure to conserve charge in a discrete PIC scheme is an entirely numerical phenomenon arising from the fact that the solution predicted by the discretized version of Ampere's law does not satisfy the discrete form of Gauss' law.

To set the stage for analysis, let us first consider the form of discrete Gauss' law, with the charge density defined as $\bar{\rho}_i(t) = [\rho_i(t), \ldots, \rho_{N_n}(t)]^T$

$$\epsilon_0[\nabla]^T[\star_\epsilon]\bar{E}(t) = \bar{\rho}(t). \tag{12}$$

To simplify the notation, we now define $\bar{\phi}(t) = \epsilon_0[\nabla]^T[\star_\epsilon]\bar{E}(t)$ to obtain

$$\bar{\phi}(t) = \bar{\rho}(t). \tag{13}$$

For the discrete solution to be consistent between Ampere's and Gauss' laws—and thereby conserve charge, we need the discrete divergence of Ampere's law to produce solutions that satisfy (12). A discrete divergence of Ampere's law gives us

$$\epsilon_0[\nabla]^T[\star_\epsilon]\partial_t\bar{E}(t) = -[\nabla]^T\bar{J}(t). \tag{14}$$

Simplifying the notation with $-[\nabla]^T \bar{J}(t) = \bar{\eta}(t)$, the divergence of discrete Ampere's law ends up as follows:

$$\partial_t \bar{\phi}(t) = \bar{\eta}(t). \tag{15}$$

Thus, for a given time-marching stencil to be innately charge conserving, the solutions produced by the discrete stencil obtained from (15) should satisfy the stencil used for (13).

1) Explicit Time Updates: EM-FEMPIC formulations described in the literature overwhelmingly adopt a leapfrog update for evolving the curl equations in time [12]. This is done for a very good reason since choosing this update scheme results in perfect compatibility between Ampere's and Gauss' laws. Applying a center-differenced leapfrog scheme at $t_{n+1/2}$ on (15) gives us

$$\frac{\bar{\phi}^{n+1} - \bar{\phi}^n}{\Delta_t} = \bar{\eta}^{n+1/2}. \tag{16}$$

Conventionally, satisfaction of (13) is usually measured pointwise at each timestep. This operation is tantamount to choosing $W_n(t) = \delta(t - t_n)$. As a result, the discrete form of Gauss' law becomes

$$\begin{aligned} &\langle \delta(t - t_n), \quad \bar{\phi}(t) = \bar{\rho}(t) \rangle \\ &\qquad \Longrightarrow \ \bar{\phi}^n = \bar{\rho}^n. \end{aligned} \tag{17}$$

Applying the same center-difference stencil to the discrete continuity equation, we obtain

$$\begin{aligned} &\bar{\eta}(t) = \partial_t \bar{\rho}(t) \\ \Longrightarrow \ &\eta^{n+1/2} = \frac{\rho^n - \rho^{n-1}}{\Delta_t}. \end{aligned} \tag{18}$$

From inspection, one can see that (18) applied to (16) results exactly in (17) so long as the initial fields in the domain satisfy Gauss' law. As a result, explicit leapfrog-based EM-FEMPIC schemes innately conserve charge.

2) Implicit Time Updates: Implicit methods, as we will shortly see, do not enforce the correspondence between the solutions obtained from Ampere's and Gauss' laws. To demonstrate this, consider (15) solved through a Newmark-β integrator [73] with $\gamma = 0.5$ and $\beta = 0.25$. In effect, the choice of γ and β fixes the representation and testing function to a set of interpolating quadratic polynomials and an average acceleration testing function. This choice of testing is consistent with choosing $W_n(t)$ as follows:

$$W_n(t) = \begin{cases} \dfrac{t_n - t}{\Delta_t}, & t \in [t_{n-1}, t_n] \\ \dfrac{t - t_n}{\Delta_t}, & t \in [t_n, t_{n+1}] \\ 0, & \text{otherwise.} \end{cases} \tag{19}$$

Applying this to (14) results in

$$\frac{\bar{\phi}^{n+1} - \bar{\phi}^{n-1}}{2} = \frac{\bar{\eta}^{n+1} + 2\bar{\eta}^n + \bar{\eta}^{n+1}}{4} \tag{20}$$

where $\bar{\eta}^n = [\nabla]^T \bar{J}^n$. To map $\bar{\eta}$ to $\bar{\rho}$, we need once again to use an integrator. As an illustration, assume that this is done using a backward Euler stencil though this analysis can be repeated with more complex stencils. Thus, applying

$$\bar{\rho}^{n+1} = \bar{\rho}^n + \Delta_t \bar{\eta^{n+1}} \tag{21}$$

to (20), we get

$$\bar{\phi}^{n+1} - \bar{\phi}^{n-1} = \frac{1}{4}\left(\bar{\rho}^{n+1} + \bar{\rho}^n - \bar{\rho}^{n-1} - \bar{\rho}^{n-2}\right). \tag{22}$$

As before, the discrete representation of (13) yields (17), which is inconsistent with (22), leading to charge not being innately conserved. We also note that, choosing a different measurement function for Gauss' law, say, the natural Newmark testing function used in Ampere's law still does not resolve the issue as

$$\frac{\bar{\phi}^{n+1} + 2\bar{\phi}^n + \bar{\phi}^{n-1}}{4} - \frac{\bar{\rho}^{n+1} + 2\bar{\rho}^n + \bar{\rho}^{n-1}}{4} = 0 \tag{23}$$

is still fundamentally incompatible with the discrete Gauss' law with different representation and measurement functions.

Getting around this problem requires a slight reformulation of Ampere's law, as demonstrated in [7]. First, consider the function $\mathbf{G}(\mathbf{r}, t)$, which denotes the time integral of the current

$$\begin{aligned} \mathbf{G}(\mathbf{r}, t) = \int_0^t \mathbf{J}(\mathbf{r}, \tau) d\tau &= q \sum_{p=1}^{N_p} \int_0^t \mathbf{v}_p(\tau) \delta(\mathbf{r} - \mathbf{r}_p(\tau)) d\tau \\ &= q \sum_{p=1}^{N_p} \int_{\mathbf{r}_p(0)}^{\mathbf{r}_p(t)} d\tilde{\mathbf{r}} \delta(\mathbf{r} - \tilde{\mathbf{r}}). \end{aligned} \tag{24}$$

Applying (24) to Ampere's law gives us

$$\nabla \times \mu_0^{-1} \mathbf{B}(\mathbf{r}, t) = \partial_t \mathbf{G}(\mathbf{r}, t) + \epsilon_0 \partial_t \mathbf{E}(\mathbf{r}, t). \tag{25}$$

Applying the spatial discretization described in V-A and applying our notational simplifications give us

$$\begin{aligned} &\langle W_n(t), \partial_t \bar{\phi}(t) = \partial_t \bar{\eta}(t) = \partial_t \bar{\rho}(t) \rangle \\ &\frac{\bar{\phi}^{n+1} - \bar{\phi}^{n-1}}{2} = \frac{\bar{\rho}^{n+1} - \bar{\rho}^{n-1}}{2} \end{aligned} \tag{26}$$

with Gauss' law as defined in (23). This time, we see that, as long as the first two initial conditions satisfy Gauss' laws pointwise, i.e., $\bar{\phi}^0 = \bar{\rho}^0$ and $\bar{\phi}^1 = \bar{\rho}^1$, (26) and (17) are exactly consistent with each other. This result holds even when replacing the testing measure with Gauss' laws with $W_a(t)$, thus enabling an implicit EM solver to be used within an FEMPIC scheme while perfectly conserving charge.

The above analysis can be trivially extended for the wave equation as done in [75].

Finally, we note that the examples shown in this section are related mainly to polynomial representations of the fields and currents. There are situations, wherein the use of other basis sets, particularly those built around complex exponential functions, is advantageous. In these situations, replacing $\bar{J}(t)$ with its time integral is not sufficient to create a scheme that perfectly conserves charge. A thorough analysis of this situation is presented in [76].

C. Havoc Due to Null Spaces in Implicit EM-FEMPIC

Null spaces always exist in implicit EM-FEMPIC. Because of this, taking a discrete divergence, as was done in Section V-B, leads to corruption of charge conservation. This

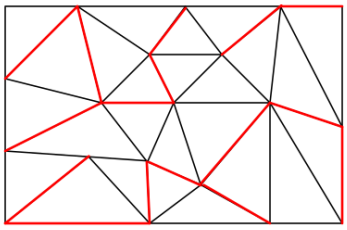

Fig. 3. Example of a 2-D mesh (bounded by nonconducting walls) with the nonsolenoidal edges (found along the minimum spanning tree) for the electric field marked in red. The remaining black edges represent the cotree unknowns.

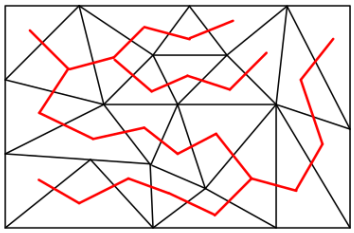

Fig. 4. Example of a mesh with the face-centered minimum spanning tree highlighted in red for the magnetic field unknowns.

corruption is of the form $\nabla\phi(\mathbf{r})$ in an implicit mixed EM-FEMPIC solver and of the form $t\nabla\phi(\mathbf{r})$ in an implicit wave equation EM-FEMPIC. This problem can be mitigated to some extent by solving for the fields at very high tolerance, with the level of spurious excitation dependent upon the tolerance used for computation. Significantly, for EM-FEMPIC, the null spaces will corrupt the satisfaction of Gauss' laws despite using the testing methods described in Section V-B. Techniques to overcome this problem are discussed next.

D. Quasi-Helmholtz or Coulomb Gauge

A robust means to satisfy Gauss' law with implicit EM-FEMPIC solvers was presented in [75]. We note that fields $\mathbf{E}(\mathbf{r},t)$ and $\mathbf{B}(\mathbf{r},t)$ can be decomposed into solenoidal and nonsolenoidal components. As a primer on notation, $\bar{E}_{ns}(t)$ refers to the nonsolenoidal coefficients of the electric field. Similarly, $\bar{E}_s(t)$ and $\bar{B}_s(t)$ refer to the solenoidal coefficients of the electric field and magnetic flux density, respectively. All relevant submatrices involved are defined entirely in Section VIII-A.

E. Projectors

Projectors to separate the nonsolenoidal components from the Whitney basis functions used in a traditional FEM solve are defined as

$$[\bar{P}]_e^{\Sigma} = \Sigma\left(\Sigma^T\Sigma\right)^{\dagger}\Sigma^T \tag{27a}$$

$$[\bar{P}]_e^{\Lambda} = \mathcal{I} - [\bar{P}]_e^{\Sigma} \tag{27b}$$

$$\left[\bar{P}\right]_b^{\Lambda} = \mathcal{I} - \Sigma_m\left(\Sigma_m^T\Sigma_m\right)^{\dagger}\Sigma_m^T \tag{27c}$$

where $\dagger$ represents a Moore–Penrose pseudoinverse, $[\Sigma] = \epsilon_0[\bar{M}_g]$ and $[\Sigma]_m = [\nabla\cdot]^T$. Numerically, this is done by separating the field unknowns using a minimum spanning tree (see Fig. 3) and its associated cotree (see Fig. 4) [66]. Applying these projectors to the field coefficients will have the effect of separating the solenoidal components as

$$\bar{D}^n = \Sigma\bar{E}_{ns}^n + \left[\bar{P}\right]_e^{\Lambda}\bar{D}^n \tag{28}$$

for the electric field and

$$\bar{B}_s^n = \left[\bar{P}\right]_b^{\Lambda}\bar{B}^n \tag{29}$$

for the magnetic flux density. By definition, the discrete divergence of the projectors is zero, and as a result, the magnetic flux density $\bar{B}^n$ will have an identically zero divergence. Note that the use of these projectors is tantamount to the imposition of the discrete Coulomb gauge. Therefore, by design, these will satisfy both Gauss' laws.

F. Discrete System

To construct a stencil from these projectors, one can apply a discrete divergence operator to (28) to obtain

$$\left[C_z^e\right]^T[\nabla]^T[\star_e][\nabla]\left[C_z^e\right]\bar{E}_{ns}(t) = -\left[C_z^e\right]^T[\nabla]^T\bar{G}(t). \tag{30}$$

Therefore, the nonsolenoidal components of the electric field can be related exactly to the charge density. The operation of (30) is the numerical analog of strongly enforcing the Coulomb gauge.

Upon using a mapping to find only the "cotree" unknowns in the mesh (which houses the solenoidal) components, these can be solved through

$$\begin{aligned}\left[\bar{Z}\right]_{11}\partial_t\bar{B}_s(t) + \left[\bar{Z}\right]_{12}\bar{E}_s(t) &= -\left[\bar{Z}\right]_{13}\bar{E}_{\mathrm{ns}}(t)\\ \left[\bar{Z}\right]_{21}\partial_t\bar{E}_s(t) - \left[\bar{Z}\right]_{22}\bar{B}_s(t) &= \bar{G}(t) - \left[\bar{Z}\right]_{23}\partial_t\bar{E}_{\mathrm{ns}}(t).\end{aligned} \tag{31}$$

The time derivatives can be evaluated by using an implicit Newmark-β operator. Note that the solutions to $\bar{E}_s(t)$ and $\bar{B}_s(t)$ will still contain null space excitations. However, when used to obtain the fields through (28) and (29), these excitations will have no influence on charge conservation.

VI. Particle Push

To evolve the particles continuously in space and time, we further need to define a particle integration or "push" scheme. Specifically, the particle motion can be obtained by solving

$$\frac{\partial\gamma[\mathbf{v}_p]\mathbf{v}_p(t)}{\partial t} = \mathbf{a}_p(t) = \frac{q}{m}\left(\mathbf{E}(\mathbf{r}_p,t) + \mathbf{v}_p\times\mathbf{B}(\mathbf{r}_p,t)\right) \tag{32a}$$

$$\frac{\partial\mathbf{r}_p(t)}{\partial t} = \mathbf{v}_p(t) \tag{32b}$$

where $\mathbf{v}_p(t)$ and $\mathbf{r}_p(t)$ are each vector in $\mathbf{R}^3$ and refer to a given particle's velocity and position, respectively, at time t. Furthermore, $\gamma[\mathbf{v}] = (1 - |\mathbf{v}|^2/c^2)$ is the relativistic time dilation functional. Many different particle integration schemes have been proposed in conjunction with EM-FEMPIC. These range from explicit or semiexplicit particle updates like the standard Boris update [8] as used in [71], or higher order Adams integrators [7], to the use of so-called kinetic enslavement schemes, where a combined monolithic EM-particle system is solved for self-consistently [87], [88] to, most recently,

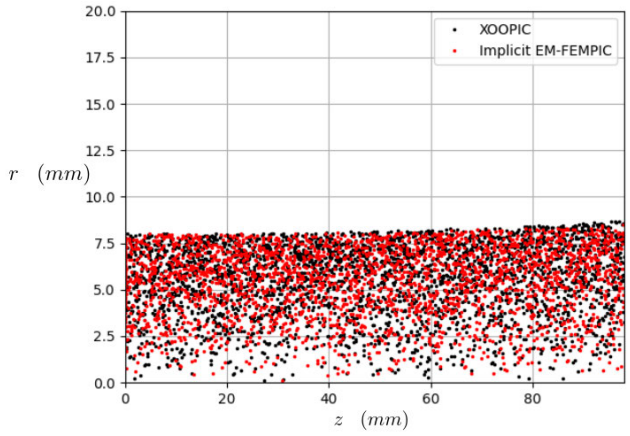

Fig. 5. Snapshot of the expanding plasma beam at $t = 5$ ns. We note that the distribution predicted by EM-FEMPIC using a fourth-order Adams integrator closely agrees with equivalent results from XOOPIC.

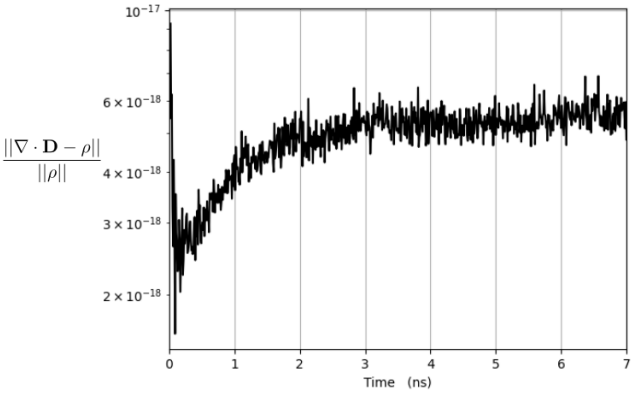

Fig. 6. Satisfaction of Gauss' law for the expanding particle beam. We note that the error is at machine precision over the course of the run.

TABLE I
PARAMETERS FOR THE EXPANDING BEAM RUN

Parameter	Value
q	1.6×10^{-19} C
m	9.1×10^{-31} kg
Beam Voltage	174 kV
Beam Current	10 A
Δ_t	10 ps
$\Delta_{t,\text{XOOPIC}}$	1 ps
N_p/timestep	50

the possibility of using predictor-corrector schemes [79]. Fundamentally, for implicit EM-FEMPIC schemes, the charge-conserving framework described for the EM system is compatible with any particle update scheme (be it explicit or predictor corrector), so long as the quantity $\mathbf{G}(\mathbf{r}, t)$ is appropriately mapped from the particle quantities through (24).

VII. NUMERICAL EXAMPLES

A. Expanding Particle Beam

To demonstrate the accuracy and function of the implicit EM-FEMPIC scheme, consider a conducting cylindrical cavity of 10 cm length and 2 cm radius oriented such that the axis of rotation was aligned along $\hat{z}$. The walls of the cavity were assumed to be perfectly conducting, and a particle beam composed of electrons was initialized at $z = 0$. The parameters

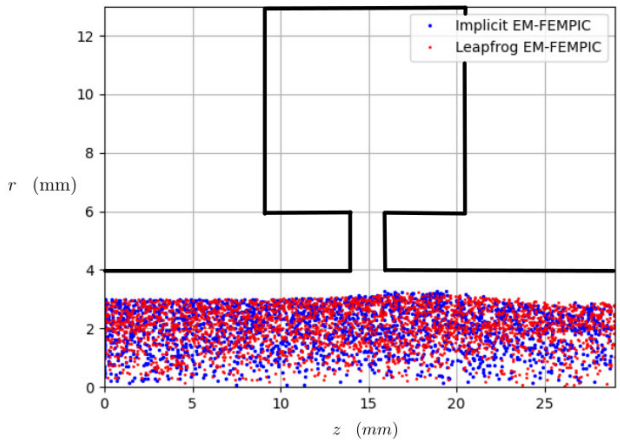

Fig. 7. Particle distribution within a cylindrical klystron at $t = 7.6$ ns. We note that the EM-FEMPIC using an energy-preserving predictor-corrector particle integrator agrees with a leapfrog-based method and exhibits particle bunching at $z \sim 20$ mm.

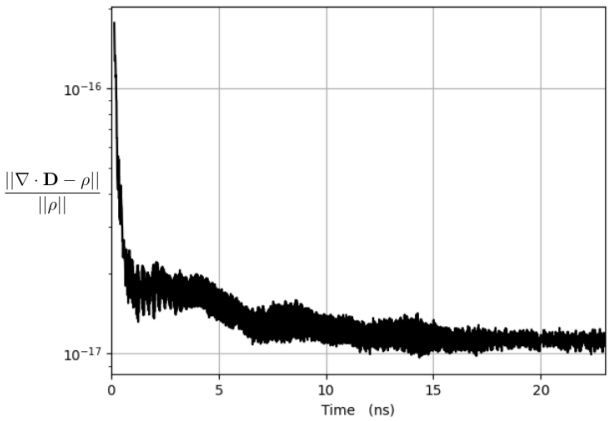

Fig. 8. Satisfaction of Gauss' law for the klystron. We note that the error is at machine precision over the course of the run.

of the simulation are given in Table I. The EM-FEMPIC simulation was formulated, as described in Section V-A-VI, and coupled with the particle push scheme described in [75]. The tetrahedral mesh used to discretize the system comprised of 3229 tetrahedra had an average edge length of 2.3 mm. A snapshot of the z–r phase space distribution particle beam at 5 ns—compared with an equivalent simulation setup on XOOPIC [89]—is reported in Fig. 5, and the satisfaction of Gauss' law over the course of the entire run is shown in Fig. 6. As is evident, the implicit method shows very good agreement with the reference method while satisfying Gauss' law to machine precision, due to the use of the quasi-Helmholtz setup described in Section V-D.

B. Particle Beam in a Klystron

Next, we considered the performance of the implicit EM-FEMPIC method to an FEMPIC method built using leapfrog by analyzing the behavior of a particle beam accelerated into a cylindrical klystron. The geometry of the device is shown in Fig. 7, with all walls assumed to be perfectly conducting. At the neck of the device ($r = 4$ mm and $z = 14 - 16$ mm), we placed a current source with a frequency of 3.9 GHz, oriented along the $\hat{z}$-direction. Once again, the system was discretized by a tetrahedral mesh comprised of

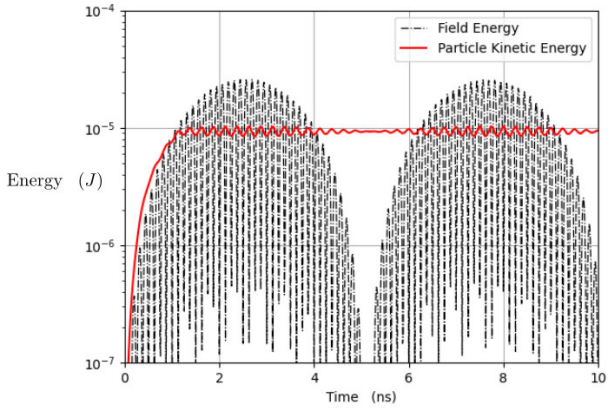

Fig. 9. Particle and field energy predicted by the implicit EM-FEMPIC case for the klystron.

TABLE II
PARAMETERS FOR THE KLYSTRON RUN

Parameter	Value
q	1.6×10^{-19} C
m	9.1×10^{-31} kg
Beam Voltage	31.05 kV
Beam Current	1 A
Δ_t	11.6 ps
$\Delta_{t,\text{Leapfrog}}$	1 ps
N_p/timestep	100

3229 tetrahedra, this time with an average edge length of 2.63 mm. The solver was run with a step size of 11.6 ps and compared to a leapfrog-based EM-FEMPIC method running at 1 ps. The parameters of the beam are reported in Table II. Once again, we note very good agreement between the implicit and explicit EM-FEMPIC implementations in Fig. 7, despite the former running at approximately 11 times the step size. Likewise, we note machine precision satisfaction of Gauss' law in Fig. 8 and good energy conservation in Fig. 9.

VIII. CONCLUSION

A thorough review of the methods and techniques used to construct EM-FEMPIC methods is discussed. Rigorous mathematical details and arguments are presented both in the construction/nuances in choosing the appropriate representation sets and in their consequences for charge conservation. We provide a detailed analysis of the challenges associated with Gauss' law satisfaction in both explicit and implicit methods and provide a description of solutions used in the current state of the art. In the course of this discussion, differences between the various solution methods were highlighted. Finally, several areas of current and future work are highlighted—these included the work on improving the accuracy and scalability of EM-FEMPIC solvers through the use of higher order representation and domain decomposition solvers, and the use of more complex particle evolution schemes and their effect on energy conservation.

APPENDIX

A. Matrix Definitions in the Quasi-Helmholtz Decomposition

To begin, the sets $\mathcal{N}$, $\mathcal{E}$, $\mathcal{F}$, and $\mathcal{T}$ are defined as the set of nodes, edges, faces, and tests, respectively, having N_n, N_f, N_e, and N_t elements. The various submatrices used in describing the quasi-Helmholtz framework in Section V-D are given as follows:

$$[\star_\epsilon]_{i,j} = \langle \mathbf{W}_i^{(1)}(\mathbf{r}), \quad \varepsilon \cdot \mathbf{W}_j^{(1)}(\mathbf{r})\rangle; i, \quad j \in \mathcal{E} \tag{33a}$$

$$\left[\star_{\mu^{-1}}\right]_{i,j} = \langle \mathbf{W}_i^{(2)}(\mathbf{r}), \quad \mu^{-1} \cdot \mathbf{W}_j^{(2)}(\mathbf{r})\rangle; \; i, j \in \mathcal{F} \tag{33b}$$

$$[\star_\rho]_{i,j} = \langle W_i^{(3)}(\mathbf{r}), \quad W_j^{(3)}(\mathbf{r})\rangle; \; i, j \in \mathcal{T} \tag{33c}$$

where $\mathbf{W}_i^{(1)}$, $\mathbf{W}_i^{(2)}$, and $W_i^{(3)}$ are the Whitney edge, face, and volume basis functions, respectively. Furthermore, we define the following matrices:

$$[\mathbf{M}_g]_{i,j} = \langle \mathbf{W}_i^{(1)}(\mathbf{r}), \quad \nabla W_j^{(0)}(\mathbf{r})\rangle; \; i \in \mathcal{E}, j \in \mathcal{N} \tag{34a}$$

$$[\mathbf{M}_c]_{i,j} = \langle \mathbf{W}_i^{(2)}(\mathbf{r}), \quad [\nabla\times]\mathbf{W}_j^{(1)}(\mathbf{r})\rangle; \; i \in \mathcal{F}, j \in \mathcal{E} \tag{34b}$$

$$[\mathbf{M}_d]_{i,j} = \langle W_i^{(3)}(\mathbf{r}), \quad [\nabla\cdot]\mathbf{W}_j^{(2)}(\mathbf{r})\rangle; \; i \in \mathcal{T}, j \in \mathcal{F} \tag{34c}$$

$$[\nabla] = \varepsilon[\star_\epsilon]^{-1}[\mathbf{M}_g] \tag{34d}$$

$$[\nabla\times] = \mu^{-1}\left[\star_{\mu^{-1}}\right]^{-1}[\mathbf{M}_c] \tag{34e}$$

$$[\nabla\cdot] = [\star_\rho]^{-1}[\mathbf{M}_d]. \tag{34f}$$

Likewise, the submatrices involved in (31) are given as follows, where the various submatrices involved in (31) are defined as:

$$[\mathbf{Z}]_{11} = \left[\mathbf{C}_c^b\right]^T [\mathbf{P}]_b^\Lambda \left[\mathbf{C}_c^b\right] \tag{35a}$$

$$[\mathbf{Z}]_{12} = \left[\mathbf{C}_c^b\right]^T [\nabla\times][\star_\varepsilon]^{-1}[\mathbf{P}]_e^\Lambda [\star_\varepsilon]\left[\mathbf{C}_c^e\right] \tag{35b}$$

$$[\mathbf{Z}]_{13} = \left[\mathbf{C}_c^b\right]^T [\nabla\times][\star_\varepsilon]^{-1}\Sigma\left[\mathbf{C}_z^e\right] \tag{35c}$$

$$[\mathbf{Z}]_{21} = \left[\mathbf{C}_c^e\right]^T [\mathbf{P}]_e^\Lambda [\star_\varepsilon]\left[\mathbf{C}_c^e\right] \tag{35d}$$

$$[\mathbf{Z}]_{22} = \left[\mathbf{C}_c^e\right]^T [\nabla\times]^T [\star_{\mu^{-1}}][\mathbf{P}]_b^\Lambda \left[\mathbf{C}_c^b\right] \tag{35e}$$

$$[\mathbf{Z}]_{23} = \left[\mathbf{C}_c^e\right]^T \Sigma\left[\mathbf{C}_z^e\right] \tag{35f}$$

where the $[C]_b$ matrices are mappings that identify unknowns that reside on the cotree. Constructing this mapping is trivial for simply connected structures but is trickier for multiply connected geometries.

ACKNOWLEDGMENT

The authors would like to acknowledge numerous discussions on the state of the art of particle-in-cell (PIC) with Dr. John Luginsland.

REFERENCES

[1] R. Marchand, "PTetra, a tool to simulate low orbit satellite–plasma interaction," *IEEE Trans. Plasma Sci.*, vol. 40, no. 2, pp. 217–229, Feb. 2012.
[2] R. W. Lemke, T. C. Genoni, and T. A. Spencer, "Three-dimensional particle-in-cell simulation study of a relativistic magnetron," *Phys. Plasmas*, vol. 6, no. 2, pp. 603–613, Feb. 1999.
[3] E. Fourkal, B. Shahine, M. Ding, J. S. Li, T. Tajima, and C.-M. Ma, "Particle in cell simulation of laser-accelerated proton beams for radiation therapy," *Med. Phys.*, vol. 29, no. 12, pp. 2788–2798, Nov. 2002.
[4] R. J. Barker and E. Schamiloglu, *High-Power Microwave Sources and Technologies*. IEEE, 2001, pp. 7–37, doi: 10.1109/9780470544877.ch2.
[5] J. J. Petillo, E. M. Nelson, J. F. DeFord, N. J. Dionne, and B. Levush, "Recent developments to the MICHELLE 2-D/3-D electron gun and collector modeling code," *IEEE Trans. Electron Devices*, vol. 52, no. 5, pp. 742–748, May 2005.
[6] C. S. Meierbachtol, A. D. Greenwood, J. P. Verboncoeur, and B. Shanker, "Conformal electromagnetic particle in cell: A review," *IEEE Trans. Plasma Sci.*, vol. 43, no. 11, pp. 3778–3793, Nov. 2015.

[7] S. O'Connor, Z. D. Crawford, O. H. Ramachandran, J. Luginsland, and B. Shanker, "Time integrator agnostic charge conserving finite element PIC," *Phys. Plasmas*, vol. 28, no. 9, Sep. 2021, Art. no. 092111.

[8] J. P. Boris, "Relativistic plasma simulation-optimization of a hybrid code," in *Proc. 4th Conf. Numer. Simulation Plasmas*, 1970, pp. 3–67.

[9] K. Yee, "Numerical solution of initial boundary value problems involving Maxwell's equations in isotropic media," *IEEE Trans. Antennas Propag.*, vol. AP-14, no. 3, pp. 302–307, May 1966.

[10] C. K. Birdsall and A. B. Langdon, *Plasma Physics Via Computer Simulation*. Boca Raton, FL, USA: CRC Press, 2004.

[11] J. Villasenor and O. Buneman, "Rigorous charge conservation for local electromagnetic field solvers," *Comput. Phys. Commun.*, vol. 69, nos. 2–3, pp. 306–316, Mar./Apr. 1992.

[12] J. P. Verboncoeur, "Particle simulation of plasmas: Review and advances," *Plasma Phys. Controlled Fusion*, vol. 47, no. 5A, pp. A231–A260, May 2005.

[13] R. Holland, "Pitfalls of staircase meshing," *IEEE Trans. Electromagn. Compat.*, vol. 35, no. 4, pp. 434–439, Nov. 1993.

[14] J. B. Schneider and K. L. Shlager, "FDTD simulations of TEM horns and the implications for staircased representations," *IEEE Trans. Antennas Propag.*, vol. 45, no. 12, pp. 1830–1838, Dec. 1997.

[15] S. Abarbanel, A. Ditkowski, and A. Yefet, "Bounded error schemes for the wave equation on complex domains," *J. Sci. Comput.*, vol. 26, no. 1, pp. 67–81, Jan. 2006, doi: 10.1007/s10915-004-4800-x.

[16] A. Akyurtlu, D. H. Werner, V. Veremey, D. J. Steich, and K. Aydin, "Staircasing errors in FDTD at an air-dielectric interface," *IEEE Microw. Guided Wave Lett.*, vol. 9, no. 11, pp. 444–446, Nov. 1999.

[17] J. P. Verboncoeur, "Aliasing of electromagnetic fields in stair step boundaries," *Comput. Phys. Commun.*, vol. 164, nos. 1–3, pp. 344–352, Dec. 2004. [Online]. Available: https://www.sciencedirect.com/science/article/pii/S0010465504003029

[18] K. Umashankar and A. Taflove, "A novel method to analyze electromagnetic scattering of complex objects," *IEEE Trans. Electromagn. Compat.*, vol. EMC-24, no. 4, pp. 397–405, Nov. 1982.

[19] A. Taflove and K. Umashankar, "A hybrid moment method/finite-difference time-domain approach to electromagnetic coupling and aperture penetration into complex geometries," *IEEE Trans. Antennas Propag.*, vol. AP-30, no. 4, pp. 617–627, Jul. 1982.

[20] K. K. Mei, A. Cangellaris, and D. J. Angelakos, "Conformal time domain finite difference method," *Radio Sci.*, vol. 19, no. 5, pp. 1145–1147, Sep. 1984, doi: 10.1029/RS019i005p01145.

[21] W. K. Gwarek, "Analysis of an arbitrarily-shaped planar circuit a time-domain approach," *IEEE Trans. Microw. Theory Techn.*, vol. MTT-33, no. 10, pp. 1067–1072, Oct. 1985.

[22] G. A. Kriegsmann, A. Taflove, and K. R. Umashankar, "A new formulation of electromagnetic wave scattering using an on-surface radiation boundary condition approach," *IEEE Trans. Antennas Propag.*, vol. AP-35, no. 2, pp. 153–161, Feb. 1987.

[23] T. G. Jurgens, A. Taflove, K. Umashankar, and T. G. Moore, "Finite-difference time-domain modeling of curved surfaces (EM scattering)," *IEEE Trans. Antennas Propag.*, vol. 40, no. 4, pp. 357–366, Apr. 1992.

[24] T. G. Jurgens and A. Taflove, "Three-dimensional contour FDTD modeling of scattering from single and multiple bodies," *IEEE Trans. Antennas Propag.*, vol. 41, no. 12, pp. 1703–1708, Jan. 1993.

[25] C. J. Railton, I. J. Craddock, and J. B. Schneider, "Improved locally distorted CPFDTD algorithm with provable stability," *Electron. Lett.*, vol. 31, no. 18, pp. 1585–1586, Aug. 1995.

[26] M. C. Marcysiak and W. K. Gwarek, "Higher-order modelling of media interfaces for enhanced FDTD analysis of microwave circuits," in *Proc. 24th Eur. Microw. Conf.*, Oct. 1994, pp. 1530–1535.

[27] N. Kaneda, B. Houshmand, and T. Itoh, "FDTD analysis of dielectric resonators with curved surfaces," *IEEE Trans. Microw. Theory Techn.*, vol. 45, no. 9, pp. 1645–1649, Sep. 1997.

[28] S. Dey, R. Mittra, and S. Chebolu, "A technique for implementing the FDTD algorithm on a nonorthogonal grid," *Microw. Opt. Technol. Lett.*, vol. 14, no. 4, pp. 213–215, May 1997.

[29] S. Dey and R. Mittra, "A locally conformal finite-difference time-domain (FDTD) algorithm for modeling three-dimensional perfectly conducting objects," *IEEE Microw. Guided Wave Lett.*, vol. 7, no. 9, pp. 273–275, Sep. 1997.

[30] S. Dey and R. Mittra, "A modified locally conformal finite-difference time-domain algorithm for modeling three-dimensional perfectly conducting objects," *Microw. Opt. Technol. Lett.*, vol. 17, no. 6, pp. 349–352, Apr. 1998.

[31] S. Dey and R. Mittra, "A conformal finite-difference time-domain technique for modeling cylindrical dielectric resonators," *IEEE Trans. Microw. Theory Techn.*, vol. 47, no. 9, pp. 1737–1739, Sep. 1999.

[32] W. Yu and R. Mittra, "A conformal FDTD software package modeling antennas and microstrip circuit components," *IEEE Antennas Propag. Mag.*, vol. 42, no. 5, pp. 28–39, Jan. 2000.

[33] I. A. Zagorodnov, R. Schuhmann, and T. A. Weiland, "A uniformly stable conformal FDTD-method in Cartesian grids," *Int. J. Numer. Model., Electron. Netw., Devices Fields*, vol. 16, no. 2, pp. 127–141, Mar. 2003.

[34] I. Zagorodnov, R. Schuhmann, and T. Weiland, "Conformal FDTD-methods to avoid time step reduction with and without cell enlargement," *J. Comput. Phys.*, vol. 225, no. 2, pp. 1493–1507, 2007.

[35] T. Xiao and Q. H. Liu, "Enlarged cells for the conformal FDTD method to avoid the time step reduction," *IEEE Microw. Wireless Compon. Lett.*, vol. 14, no. 12, pp. 551–553, Dec. 2004.

[36] T. Xiao and Q. H. Liu, "A 3-D enlarged cell technique (ECT) for the conformal FDTD method," *IEEE Trans. Antennas Propag.*, vol. 56, no. 3, pp. 765–773, Mar. 2008.

[37] Y. Wang, J. Wang, Z. Chen, G. Cheng, and P. Wang, "Three-dimensional simple conformal symplectic particle-in-cell methods for simulations of high power microwave devices," *Comput. Phys. Commun.*, vol. 205, pp. 1–12, Aug. 2016. [Online]. Available: https://www.sciencedirect.com/science/article/pii/S0010465516300650

[38] N. K. Madsen and R. W. Ziolkowski, "A three-dimensional modified finite volume technique for Maxwell's equations," *Electromagnetics*, vol. 10, nos. 1–2, pp. 147–161, Jan. 1990.

[39] V. Shankar, A. H. Mohammadian, and W. F. Hall, "A time-domain, finite-volume treatment for the Maxwell equations," *Electromagnetics*, vol. 10, nos. 1–2, pp. 127–145, 1990.

[40] A. H. Mohammadian, V. Shankar, and W. F. Hall, "Computation of electromagnetic scattering and radiation using a time-domain finite-volume discretization procedure," *Comput. Phys. Commun.*, vol. 68, nos. 1–3, pp. 175–196, Nov. 1991.

[41] R. Holland, V. P. Cable, and L. C. Wilson, "Finite-volume time-domain (FVTD) techniques for EM scattering," *IEEE Trans. Electromagn. Compat.*, vol. 33, no. 4, pp. 281–294, Nov. 1991.

[42] S. D. Gedney and F. Lansing, "A parallel discrete surface integral equation method for the analysis of three-dimensional microwave circuit devices with planar symmetry," in *Proc. IEEE Antennas Propag. Soc. Int. Symp., URSI Nat. Radio Sci. Meeting*, Seattle, WA, USA, vol. 3, 1994, pp. 1778–1781, doi: 10.1109/APS.1994.408194.

[43] N. K. Madsen, "Divergence preserving discrete surface integral methods for Maxwell's curl equations using non-orthogonal unstructured grids," *J. Comput. Phys.*, vol. 119, no. 1, pp. 34–45, 1995. [Online]. Available: https://www.sciencedirect.com/science/article/pii/S002199918571114X

[44] F. Hermeline, "A finite volume method for solving Maxwell equations in inhomogeneous media on arbitrary meshes," *Comp. Rendus Mathematique*, vol. 339, no. 12, pp. 893–898, Dec. 2004. [Online]. Available: https://www.sciencedirect.com/science/article/pii/S1631073X04004546

[45] M. Matsumoto and S. Kawata, "TRIPIC: Triangular-mesh particle-in-cell code," *J. Comput. Phys.*, vol. 87, no. 2, pp. 488–493, Apr. 1990. [Online]. Available: https://www.sciencedirect.com/science/article/pii/002199919090262Y

[46] A. M. Winslow, "Numerical solution of the quasilinear Poisson equation in a nonuniform triangle mesh," *J. Comput. Phys.*, vol. 135, no. 2, pp. 128–138, Aug. 1997. [Online]. Available: https://www.sciencedirect.com/science/article/pii/S0021999197956989

[47] G. Lapenta, F. Iinoya, and J. U. Brackbill, "Particle-in-cell simulation of glow discharges in complex geometries," *IEEE Trans. Plasma Sci.*, vol. 23, no. 4, pp. 769–779, Aug. 1995.

[48] C.-D. Munz, P. Omnes, R. Schneider, E. Sonnendrücker, and U. Voß, "Divergence correction techniques for Maxwell solvers based on a hyperbolic model," *J. Comput. Phys.*, vol. 161, pp. 484–511, Jul. 2000.

[49] C.-D. Munz et al., "KAD12D-a particle-in-cell code based on finite-volume methods," in *Proc. 12th Int. Conf. High-Power Part. Beams. (BEAMS)*, Jun. 1998, pp. 541–544.

[50] C. Munz, R. Schneider, E. Sonnendrücker, E. Stein, U. Voss, and T. Westermann, "A finite-volume particle-in-cell method for the numerical treatment of Maxwell–Lorentz equations on boundary-fitted meshes," *Int. J. Numer. Methods Eng.*, vol. 44, no. 4, pp. 461–487, Feb. 1999.

[51] N. Gatsonis and A. Spirkin, "Unstructured 3D simulations of field emission array cathodes for micropropulsion applications," in *Proc. 38th AIAA/ASME/SAE/ASEE Joint Propuls. Conf. Exhib.*, Jul. 2002, p. 3687, doi: 10.2514/6.2002-3687.

[52] A. Spirkin and N. Gatsonis, "Unstructured 3D PIC simulation of plasma flow in a segmented microchannel," in *Proc. 36th AIAA Thermophys. Conf.*, Jul. 2003, p. 3896, doi: 10.2514/6.2003-3896.

[53] A. Spirkin and N. A. Gatsonis, "Unstructured 3D PIC simulations of the flow in a retarding potential analyzer," *Comput. Phys. Commun.*, vol. 164, no. 1, pp. 383–389, 2004. [Online]. Available: https://www.sciencedirect.com/science/article/pii/S0010465504003078

[54] J. S. Hesthaven and T. Warburton, "Nodal high-order methods on unstructured grids: I. Time-domain solution of Maxwell's equations," *J. Comput. Phys.*, vol. 181, no. 1, pp. 186–221, 2002. [Online]. Available: https://www.sciencedirect.com/science/article/pii/S0021999102971184

[55] M. Movahhedi, A. Abdipour, A. Nentchev, M. Dehghan, and S. Selberherr, "Alternating-direction implicit formulation of the finite-element time-domain method," *IEEE Trans. Microw. Theory Techn.*, vol. 55, no. 6, pp. 1322–1331, Jun. 2007.

[56] S. Piperno and L. F. Fezoui, "A centered discontinuous Galerkin finite volume scheme for the 3D heterogeneous Maxwell equations on unstructured meshes," INRIA, Tech. Rep. RR-4733, Feb. 2003. [Online]. Available: https://hal.inria.fr/inria-00071854

[57] A. Taube, M. Dumbser, C.-D. Munz, and R. Schneider, "A high-order discontinuous Galerkin method with time-accurate local time stepping for the Maxwell equations," *Int. J. Numer. Modelling, Electron. Netw., Devices Fields*, vol. 22, no. 1, pp. 77–103, Jan. 2009, doi: 10.1002/jnm.700.

[58] G. B. Jacobs and J. S. Hesthaven, "High-order nodal discontinuous Galerkin particle-in-cell method on unstructured grids," *J. Comput. Phys.*, vol. 214, no. 1, pp. 96–121, May 2006. [Online]. Available: https://www.sciencedirect.com/science/article/pii/S0021999105004250

[59] G. Jacobs, J. Hesthaven, and G. Lapenta, "Simulations Weibel instability with a high-order discontinous Galerkin particle-in-cell solver," in *Proc. 44th AIAA Aerospace Sci. Meeting Exhib.*, 2006, p. 1171, doi: 10.2514/6.2006-1171.

[60] G. B. Jacobs and J. S. Hesthaven, "Implicit–explicit time integration of a high-order particle-in-cell method with hyperbolic divergence cleaning," *Comput. Phys. Commun.*, vol. 180, no. 10, pp. 1760–1767, Oct. 2009. [Online]. Available: https://www.sciencedirect.com/science/article/pii/S0010465509001490

[61] R. E. Heath, "Analysis of the discontinuous Galerkin method applied to collisionless plasma physics," Ph.D. dissertation, Dept. Comput. Appl. Math., Univ. Texas, Austin, TX, USA, Jan. 2007.

[62] J. A. Rossmanith and D. C. Seal, "A positivity-preserving high-order semi-Lagrangian discontinuous Galerkin scheme for the Vlasov–Poisson equations," *J. Comput. Phys.*, vol. 230, no. 16, pp. 6203–6232, Jul. 2011. [Online]. Available: https://www.sciencedirect.com/science/article/pii/S0021999111002579

[63] B. Ayuso, J. A. Carrillo, and C.-W. Shu, "Discontinuous Galerkin methods for the one-dimensional Vlasov–Poisson system," *Kinetic Rel. Models*, vol. 4, no. 4, pp. 955–989, 2011. [Online]. Available: article/id/343c512f-d0f8-4b78-ba9c-cf4ceb62ddca

[64] Y. Cheng, I. M. Gamba, F. Li, and P. J. Morrison, "Discontinuous Galerkin methods for the Vlasov–Maxwell equations," *SIAM J. Numer. Anal.*, vol. 52, no. 2, pp. 1017–1049, Jan. 2014, doi: 10.1137/130915091.

[65] Y. Cheng, A. J. Christlieb, and X. Zhong, "Energy-conserving discontinuous Galerkin methods for the Vlasov–Ampère system," *J. Comput. Phys.*, vol. 256, pp. 630–655, Jan. 2014. [Online]. Available: https://www.sciencedirect.com/science/article/pii/S0021999113006189

[66] J.-M. Jin, *The Finite Element Method in Electromagnetics*. Hoboken, NJ, USA: Wiley, 2015.

[67] M. C. Pinto, S. Jund, S. Salmon, and E. Sonnendrucker, "Charge-conserving FEM–PIC schemes on general grids," *Comptes Rendus Mécanique*, vol. 342, no. 10, pp. 570–582, 2014.

[68] H. Moon, F. L. Teixeira, and Y. A. Omelchenko, "Exact charge-conserving scatter–gather algorithm for particle-in-cell simulations on unstructured grids: A geometric perspective," *Comput. Phys. Commun.*, vol. 194, pp. 43–53, Sep. 2015.

[69] J. Squire, H. Qin, and W. M. Tang, "Geometric integration of the Vlasov–Maxwell system with a variational particle-in-cell scheme," *Phys. Plasmas*, vol. 19, no. 8, Aug. 2012, Art. no. 084501.

[70] S. O'Connor, Z. D. Crawford, J. Verboncoeur, J. Lugisland, and B. Shanker, "A set of benchmark tests for validation of 3D particle in cell methods," 2021, *arXiv:2101.09299*.

[71] M. Kraus, K. Kormann, P. J. Morrison, and E. Sonnendrücker, "GEMPIC: Geometric electromagnetic particle-in-cell methods," *J. Plasma Phys.*, vol. 83, no. 4, Aug. 2017, Art. no. 905830401.

[72] J. Xiao, H. Qin, and J. Liu, "Structure-preserving geometric particle-in-cell methods for vlasov-maxwell systems," *Plasma Sci. Technol.*, vol. 20, no. 11, Nov. 2018, Art. no. 110501.

[73] O. C. Zienkiewicz, "A new look at the Newmark, Houbolt and other time stepping formulas. A weighted residual approach," *Earthq. Eng. Struct. Dyn.*, vol. 5, no. 4, pp. 413–418, Oct. 1977.

[74] Z. D. Crawford, S. O'Connor, J. Luginsland, and B. Shanker, "Rubrics for charge conserving current mapping in finite element particle in cell methods," 2021, *arXiv:2101.12128*.

[75] S. O'Connor, Z. D. Crawford, O. H. Ramachandran, J. Luginsland, and B. Shanker, "Quasi–Helmholtz decomposition, Gauss' laws and charge conservation for finite element particle-in-cell," *Comput. Phys. Commun.*, vol. 276, p. 108345, 2022. [Online]. Available: https://www.sciencedirect.com/science/article/pii/S0010465522000637, doi: 10.1016/j.cpc.2022.108345.

[76] O. H. Ramachandran, Z. D. Crawford, S. O'Connor, J. Luginsland, and B. Shanker, "An envelope tracking approach for particle in cell simulations," 2022, *arXiv:2208.12795*.

[77] Z. D. Crawford, O. H. Ramachandran, S. O'Connor, J. Luginsland, and B. Shanker, "Higher order charge conserving electromagnetic finite element particle in cell method," 2021, *arXiv:2111.12411*.

[78] Z. D. Crawford, O. H. Ramachandran, S. O'Connor, D. L. Dault, J. Luginsland, and B. Shanker, "Domain decomposition framework for Maxwell finite element solvers and application to PIC," 2022, *arXiv:2204.13254*.

[79] O. H. Ramachandran, L. C. Kempel, J. Luginsland, and B. Shanker, "A charge conserving exponential predictor corrector FEMPIC formulation for relativistic particle simulations," 2023, *arXiv:2303.08037*.

[80] J. Xiao and H. Qin, "Explicit structure-preserving geometric particle-in-cell algorithm in curvilinear orthogonal coordinate systems and its applications to whole-device 6D kinetic simulations of Tokamak physics," *Plasma Sci. Technol.*, vol. 23, no. 5, May 2021, Art. no. 055102.

[81] A. S. Glasser and H. Qin, "The geometric theory of charge conservation in particle-in-cell simulations," 2019, *arXiv:1910.12395*.

[82] A. Bossavit, "Whitney forms: A class of finite elements for three-dimensional computations in electromagnetism," *IEE Proc. A, Phys. Sci., Meas. Instrum., Manage. Educ.-Rev.*, vol. 135, no. 8, pp. 493–500, Nov. 1988.

[83] Z. Crawford, J. Li, A. Christlieb, and B. Shanker, "Unconditionally stable time stepping method for mixed finite element Maxwell solvers," *Prog. Electromagn. Res. C*, vol. 103, pp. 17–30, 2020.

[84] M. F. Wong, O. Picon, and V. Fouad Hanna, "A finite element method based on Whitney forms to solve Maxwell equations in the time domain," *IEEE Trans. Magn.*, vol. 31, no. 3, pp. 1618–1621, May 1995.

[85] B. He and F. L. Teixeira, "Geometric finite element discretization of Maxwell equations in primal and dual spaces," *Phys. Lett. A*, vol. 349, pp. 1–14, Jan. 2006.

[86] A. Bossavit and L. Kettunen, "Yee-like schemes on a tetrahedral mesh, with diagonal lumping," *Int. J. Numer. Model., Electron. Netw., Devices Fields*, vol. 12, nos. 1–2, pp. 129–142, 1999.

[87] S. Markidis and G. Lapenta, "The energy conserving particle-in-cell method," *J. Comput. Phys.*, vol. 230, no. 18, pp. 7037–7052, Aug. 2011. [Online]. Available: https://www.sciencedirect.com/science/article/pii/S0021999111003445

[88] S. Markidis, "Development of implicit kinetic simulation methods, and their application to ion beam propagation in current and future neutralized drift compression experiments," Ph.D. dissertation, Dept. Nucl., Plasma Radiol. Eng., Univ. Illinois at Urbana-Champaign, Champaign, IL, USA, 2010. [Online]. Available: https://hdl.handle.net/2142/16090

[89] J. P. Verboncoeur, A. B. Langdon, and N. T. Gladd, "An object-oriented electromagnetic PIC code," *Comput. Phys. Commun.*, vol. 87, nos. 1–2, pp. 199–211, 1995. [Online]. Available: https://www.sciencedirect.com/science/article/pii/001046559400173Y

Omkar H. Ramachandran (Graduate Student Member, IEEE) received the B.A. degree in physics from the University of Colorado Boulder, Boulder, CO, USA, in 2018. He is currently pursuing the Ph.D. degree in electrical and computer engineering with Michigan State University, East Lansing, MI, USA.

His research interests include several topics in computational electromagnetics, including particle-in-cell methods, analysis of coupled EM-device systems, and nonlinear optimization.

Leo C. Kempel (Fellow, IEEE) was born in Akron, OH, USA, in 1965. He received the B.S.E.E. degree from the University of Cincinnati, Cincinnati, OH, USA, in 1989, and the M.S.E.E. and Ph.D. degrees from the University of Michigan, Ann Arbor, MI, USA, in 1990 and 1994, respectively.

After a brief post-doctoral appointment at the University of Michigan, he joined Mission Research Corporation, Goleta, CA, USA, in 1994, as a Senior Research Engineer. He led several projects involving the design of conformal antennas, computational electromagnetics, scattering analysis, and high-power/ultrawideband microwaves. He joined Michigan State University, East Lansing, MI, USA, in 1998. He was an Intergovernmental Personnel Act (IPA) with the Air Force Research Laboratory's Sensors Directorate, Riverside, OH, USA, from 2004 to 2005 and 2006 to 2008. He was the Inaugural Director of the Michigan State University High Performance Computing Center, East Lansing. He was the first Associate Dean for Special Initiatives of the College of Engineering, Michigan State University, from 2006 to 2008, where he was the Associate Dean for Research from 2008 to 2013 and then became the Acting Dean of Engineering in 2013. Since 2014, he has been the Dean of the College of Engineering, Michigan State University. He has coauthored the book *Finite Element Method for Electromagnetics* (IEEE Press). His current research interests include computational electromagnetics, conformal antennas, microwave/millimeter-wave materials, and measurement techniques.

Prof. Kempel was a member of the Antennas and Propagation Society's Administrative Committee and the ACES Board of Directors. He is a member of Tau Beta Pi, Eta Kappa Nu, and Commission B of URSI. He is a fellow of the Applied Computational Electromagnetics Society (ACES). He was a recipient of the CAREER Award by the National Science Foundation, the Teacher-Scholar Award by Michigan State University in 2002, and the MSU College of Engineering's Withrow Distinguished Scholar (Junior Faculty) Award in 2001. He has served as the Technical Chairperson for the 2001 ACES Conference and the Technical Co-Chair of the Finite Element Workshop held in Chios, Greece, in 2002. He was the Fellow Evaluation Committee Chairperson for the IEEE Antennas and Propagation Society and has served on the IEEE Fellow Board from 2013 to 2015. He has served on the U.S. Air Force Scientific Advisory Board from 2011 to 2015. He has served as an Associate Editor of the IEEE TRANSACTIONS ON ANTENNAS AND PROPAGATION. He is an Active Reviewer of several IEEE publications and the *Journal of Electromagnetic Waves and Applications* and *Radio Science*.

John P. Verboncoeur (Fellow, IEEE) received the B.S. degree from the University of Florida, Gainesville, FL, USA, in 1986, and the M.S. and Ph.D. degrees in nuclear engineering from the University of California at Berkeley (UCB), Berkeley, CA, USA, in 1987 and 1992, respectively.

Following appointments as a Post-Doctoral Researcher at UCB and the Lawrence Livermore National Laboratory, Livermore, CA, USA, and a Research Engineer at UCB, he joined the UCB Nuclear Engineering Faculty in 2001, where he chaired the Computational Engineering Science Program from 2001 to 2010. In 2011, he was appointed as a Professor of electrical and computer engineering at Michigan State University (MSU), East Lansing, MI, USA. He is currently an Acting Associate Dean for Research of the College of Engineering, MSU. He has authored/coauthored over 400 journal articles and conference papers, with about 5000 citations, and has taught 13 international workshops and minicourses on plasma simulation. His research interests are in theoretical and computational plasma physics and applications.

Prof. Verboncoeur is a member of the American Physical Society Division of Plasma Physics. He is the Past President of the IEEE Nuclear and Plasma Sciences Society, and the Past IEEE Director and the Past Acting VP of the IEEE Publications, Services, and Products Board. He also serves on the Board of Directors of the American Center for Mobility National Proving Ground. He is an Associate Editor of *Physics of Plasmas* and serves on the DOE Fusion Energy Sciences Advisory Committee.

B. Shanker (Fellow, IEEE) received the B.Tech. degree from IIT Madras, Chennai, India, in 1989, and the M.S. and Ph.D. degrees from The Pennsylvania State University, State College, PA, USA, in 1992 and 1993, respectively.

From 1993 to 1996, he was a Research Associate with the Department of Biochemistry and Biophysics, Iowa State University, Ames, IA, USA, where he worked on the Molecular Theory of Optical Activity. From 1996 to 1999, he was a Visiting Assistant Professor with the Center for Computational Electromagnetics, University of Illinois at Urbana–Champaign, Champaign, IL, USA. From 1999 to 2002, he was an Assistant Professor with the Department of Electrical and Computer Engineering (ECE), Iowa State University. Since 2017, he has been a University Distinguished Professor (an honor accorded to about 2% of tenure system MSU faculty members) with the Department of ECE and the Department of Physics and Astronomy, Michigan State University (MSU), East Lansing, MI, USA. He has served as the Associate Chair for Graduate Studies at the Department of ECE, MSU, from 2012 to 2015, where he was the Associate Chair for Research in ECE from 2019 to 2022. He is currently a Professor and the Chair of ECE with The Ohio State University, Columbus, OH, USA. At MSU, he was appointed as the Associate Chair of the Department of Computational Mathematics, Science and Engineering, a new department at MSU, and was a key player in building this department. He has authored/coauthored around 450 journal articles and conference papers, and presented a number of invited talks. His research interests include all aspects of computational electromagnetics (frequency- and time-domain integral equation-based methods, multiscale fast multipole methods, fast transient methods, higher order finite element, and integral equation methods), propagation in complex media, mesoscale electromagnetics, and particle and molecular dynamics as applied to multiphysics and multiscale problems.

Dr. Shanker is a Full Member of the USNC-URSI Commission B. He is a fellow of IEEE (class 2010), elected for his contributions to time- and frequency-domain computational electromagnetics. He has been awarded the Withrow Distinguished Junior Scholar in 2003, the Withrow Distinguished Senior Scholar in 2010, the Withrow Teaching Award in 2007, and the Beal Outstanding Faculty Award in 2014. He was an Associate Editor of IEEE ANTENNAS AND WIRELESS PROPAGATION LETTERS (AWPL) and IEEE TRANSACTIONS ON ANTENNAS AND PROPAGATION and a Topical Editor of *Journal of the Optical Society of America A*.